Received: 4 January 2021 | Revised: 23 February 2021 | Accepted: 5 March 2021

DOI: 10.1002/vnl.21821

RESEARCH ARTICLE

JOURNAL OF Vinyl & Additive TECHNOLOGY WILEY

Application of graphene-based adsorbents in the treatment of dye-contaminated wastewater; kinetic and isotherm studies

Ferda Mindivan[1] | **Ülküye Dudu Gül**[2] | **Meryem Göktaş**[3]

[1]Faculty of Engineering, Department of Bioengineering, Bilecik Seyh Edebali University, Bilecik, Turkey

[2]Vocational School of Health Services, Bilecik Seyh Edebali University, Bilecik, Turkey

[3]Vocational College, Department of Metallurgy, Bilecik Seyh Edebali University, Bilecik, Turkey

Correspondence
Ferda Mindivan, Bilecik Seyh Edebali University, Faculty of Engineering, Department of Bioengineering, Bilecik, 11230, Turkey.
Email: ferda.mindivan@bilecik.edu.tr

Abstract

The adsorption of methylene blue (MB) on graphene-based adsorbents was tested through the batch experimental method. Two types of graphene-based adsorbents as graphene oxide (GO) and reduced graphene oxide (RGO) were compared to investigate the best adsorbent for MB removal. So that optimizing the MB removal for the selected type of graphene-based adsorbent, the diverse experimental factors, as pH (2–10), contact time (0–1440 min), adsorbent dosage (0.5–2 g/L), and initial MB concentration (25–400 mg/L) were analyzed. The conclusions indicated that the MB removal rised with an increase in the initial concentration of the MB and so rises in the amount of adsorbent used and initial pH. Maximum dye removal was calculated as 99.11% at optimal conditions after 240 min. Adsorption data were compiled by the Langmuir isotherm (R^2: 0.999) and pseudo-second-order kinetic models (R^2: 0.999). The Langmuir isotherm model accepted that the homogeneous surface of the GO adsorbent covering with a single layer. And the adsorption energy was calculated as 9.38 kJ mol^{-1} according to the D-R model indicating the chemical adsorption occurred. The results show that GO could be utilized for the treatment of dye-contaminated aqueous solutions effectively.

KEYWORDS

adsorption, adsorption kinetics, graphene oxide, methylene blue, reduced graphene oxide

1 | INTRODUCTION

The quality of water is a very important constituent of our ecosystem.[1] Water pollution is one of the best pressing troubles all over the world[2] and sufficient data are not available about new emerging pollutants.[3,4,5,6] Dyes are extensively used in industrial applications and also, caused water pollution problems owing to the presence in the wastewater of these applications.[2,7] It is reported that 10%–15% of dyes were joined to the wastewater of fabrics, then discharged to the environment.[2] Some physical, chemical, and biological techniques including fenton oxidation, membrane filtration, and adsorption are used for the decontaminate wastewater that has dye.[8–9] In these techniques, adsorption is preferred among the other processes because of its inexpensive nature.[10–11] Recently, researches are focused on determining the most suitable and efficient adsorbent used in the adsorption process.[12–15] Different adsorbents for methylene blue (MB) removal were used such as agricultural wastes, plant solid wastes, biomass, clays

minerals and zeolites, and some of them showed good MB adsorption quality.[16] Graphene oxide (GO) is suggested as an environmentally friendly candidate to take out of dyes from aqueous solutions due to its relative biocompatibility.[17–19] Graphene and its derivatives, particularly GO and reduced graphene oxide (RGO), have been extensively used in the areas of science and technology because of their large surface area, possible further functionalization, free π–π electron and reactive functional groups, biocompatibility, and low toxicity.[20–22] GO and RGO is often prepared by the top–down strategy because this method uses for wide-reaching manufacture of graphene derivatives exhibiting major economic advantage.[23] GO consists of carboxyl (COOH) groups and carbonyl (—C═O) groups at the sheet edges, epoxy (C—O—C) groups, and hydroxyl (—OH) groups on the basic plane and RGO has carboxyl (COOH) and hydroxyl (—OH) groups on their edges and basal planes. Therefore, they are hydrophilic, can be well dispersed in aqueous solutions.[24–25] These properties of GO and RGO have promising potential for environment-friendly and effective approaches in the fields of adsorption research. Arabpour et al.[26] reported the effect of the synthesize reaction condition of GO, Ferreira et al.[27] prepared RGO-zinc oxide (rGO-ZnO) composite, Jiang et al.[28] constructed a cross-linked graphene aerogel, Rohaizad et al.[29] synthesized silver nanoparticles from *Catharanthus roseus* (*C. roseus*) dried peels extract doped with GO, Calimli et al.[30] used RGO-supported Ni nanoadsorbents for the removal of MB at the last manuscripts. Wang et al.[31] and Xu et al.[32] investigated effective adsorption of MB from aqueous solution to GO-modified persimmon tannins and triethanolamine-modified GO. Lokhande et al.[33] synthesized a new adsorbent, the combination of GO, alkyd resin, and silica nanoparticles to suspend the MB from aqueous. Pethsangave et al.[34] presented an easy and productive synthesis of nanocomposite samples of magnetic detachable graphene polyaniline-ferrite and graphene polypyrrole-ferrite for photocatalytic use dye degradation of pollutants. However, available literature contains limited amounts of studies including the isotherm and kinetic modeling of dye adsorption by GO. Also, in this paper, RGO is produced by vitamin C (ascorbic acid) and according to our knowledge, no information about adsorption studies of RGO is produced by vitamin C. This study aims to establish the potential application of graphene-basic adsorbents (Graphite [G], GO, and RGO) in the treatment of MB dye-contaminated wastewater. The results of this study suggested that the use of GO compared to G and RGO in dye polluted water resources.

2 | EXPERIMENTAL

2.1 | Preparation of adsorbents

Natural graphite (45 μm nominal particle size, ≥99.99% trace metals basis, CAS Number 7782-42-5) powder (G), concentrated sulfuric acid (98% H_2SO_4), potassium permanganate ($KMnO_4$), hydrochloric acid (HCI), hydrogen peroxide (30% H_2O_2), and vitamin C (L[+]-ascorbic acid) were provided from Merck. All the reagents were used without further refinement. The GO powder synthesis from G was obtained using the modified Hummer's method.[35] G (3 g) and concentrated H_2SO_4 (207 ml) was mixed into a circular bottom flask. The mixture was held on an ice bath for 30 min. Subsequently, $KMnO_4$ (24 g) was progressively added with stable stirring in an ice bath to avoid an instantaneous increase in temperature and the reaction mixture was stirred for 15 min. The ice bath was then taken and the mixture was stirred at 35°C one-night to form a thickened paste. Subsequently, 210 ml deionized water was added stepwise, and the mixture was stirred at 98°C for about 2 h. About 36 ml of H_2O_2 (30 wt%) solution was added to the mixture and the solution color turned into golden yellow instantly. Eventually, the mixture was after that filtered and washed more than once together with 3% HCl and deionized water up to pH 7 and dehydrated at 65°C for 12 h to get GO powders. The RGO powder was prepared using the method reported in our previous works.[36]

2.2 | Characterization of adsorbent

Structural analyses of the GO and MB-treated GO (MB-GO) were obtained by Fourier transformed infrared spectroscopy (FTIR) spectra (Spectrum 100, Perkin Elmer) 4000–400 cm^{-1} of range. The crystalline structure of samples was examined by X-ray diffraction (XRD) using Cu Kα radiation (λ = 1.5404 Å) in the 2θ range of 5.0–60° with a step size of 0.1° to measure the interlayer distance for both samples. XRD data were provided by a PAN analytical Empyrean diffractometer. The surface morphology was analyzed by a scanning electron microscopy (SEM, Supra 40VP, Zeiss). Energy-dispersive X-ray spectroscopy (EDS) analysis was also performed on the same device.

2.3 | Preparation of dye solution

The cationic dye called MB was provided from Merck. The stock dye solution was prepared by dissolving in

deionized water at a concentration of 2.0% (wt/vol). Experimental arrangements were prepared by adding the desired amounts of this stock solution into the working solutions.

2.4 | Dye removal experiments

Dye removal studies were realized by the batch technique in 50 ml bottles containing MB including synthetic solutions at the wanted level of every component at the starting of the adsorption. The flasks were regularly agitated on a shaker at stable shaking rate of 100 rpm for 24 h to provide that balance was reached. To determine the effect of adsorbent type on MB adsorption, the different types of adsorbent (Dry weight: 1 g/L) were added into flasks that contained 50 ml deionized water with 50 mg/L MB at pH 7.05 for 0–1440 min. To examine the effect of initial MB concentrations on adsorption, the adsorbent was added into flasks that contained distilled water with 25, 50, 100, 200, and 400 mg/L MB. The effect of pH was detected in flasks that contained distilled water with 25 mg/L MB at pH 2, 4, 6, 8, and 10. To investigate the effect of adsorbent dosage 0.5, 1, and 2 g/L dosages of adsorbents were added into the flasks containing 50 ml of deionized water with 50 mg/L MB dye. The effect of contact time was tested with samples taken at certain periods such as 0, 30, 45, 60, 90, 120, 150, 180, 240, 360, 420, and 1440 min. The 50 ml distilled water flask containing only MB without adsorbent was used as a control. The experiments were repeated four times and the averages were used and also, the standard deviations were calculated.

2.5 | Dye removal analysis

Samples (1 ml) were taken at a certain period, and then centrifuged at 10000 rpm for 7 min (Hettich EBTA12 model centrifuge). The supernatants were analyzed at 665 nm wavelength by spectrophotometric method. During the spectrophotometric analysis, the flasks that contained distilled water were used as controls. Absorbance measurements and centrifugation were realized using a Thermoscientific, Genesys 150 UV–Vis spectrophotometer, and Hettich EBTA12 model centrifuge device, respectively. The percentage adsorption of dye was calculated from;

$$\mathrm{DR}\,(\%) = (\mathrm{C_o} - \mathrm{C_f})/\mathrm{C_o}\,\mathrm{x}\,100. \quad (1)$$

The dye uptake capacity of adsorbent is calculated based on the mass balance principle from;

$$q_m = (\mathrm{C_o} - \mathrm{C_f})/\mathrm{X_m}. \quad (2)$$

In these equations; DR (%) is the percentage of dye removal rate, q_m is the maximum specific dye uptake (mg/g), X_m is the maximum dried cell mass (g/L), Co is the initial dye concentration (mg/L), and C_f is the final dye concentration (mg/L).

2.6 | Adsorption isotherm and kinetics

The frequently used isotherm models called Freundlich, Langmuir, and Dubinin–Radushkevich (D–R) were calculated using the results of experiments at optimal conditions.

The isotherm equations were calculated from Equations (3) and (4).

$$\mathrm{C_e}/q_e = (1/q_m)\mathrm{C_e} + 1/\mathrm{K_{Lqm}}. \quad (3)$$

Langmuir isotherm equation.

$$\ln(qe) = \ln(\mathrm{KF}) + 1/\mathrm{n}\ln(\mathrm{C_e}). \quad (4)$$

Freundlich isotherm equation.

$$\mathrm{q} = \mathrm{X_{DRe}} - \mathrm{K_{DR}}^{\varepsilon 2}. \quad (5)$$

Dubinin-Radushkevich (D-R) equation.

$$\varepsilon = \mathrm{RT}\,(\ln 1 + 1/\mathrm{ce}). \quad (6)$$

Polanyi potential calculation in D-R.

$$\mathrm{E} = (2\mathrm{K_{DR}})^{-0.3}. \quad (7)$$

Adsorption free energy calculation in D-R.In these equations; *qe*: the amount of dye adsorbed per unit weight of adsorbent at equilibrium (mg/g), *qm*: the maximum dye uptake per unit mass of adsorbent (mg/g), K_L: the Langmuir isotherm constant (L/mg), K_F: the Freundlich isotherm constant (L/mg), q: the amount of adsorbed MB dye (mol kg^{-1}) in D-R equation, X_{DR}: adsorption capacity, K_{DR}: a measure of activity coefficient (mol^2 K J^2), ε: Polanyi potential, R: the ideal gas constant (8.314 J mol^{-1} K^{-1}), T (K): the absolute temperature, E: adsorption free energy (kJ mol^{-1}).

To examine the kinetics of the MB dye adsorption in terms of the theoretical *qe* values and order of rate constant, pseudo-first-order and pseudo-second-order kinetic model equations were used. Kinetic data were calculated with the equations;

$$\log(qe - qt) = -k_1/2.303t + \log qe. \quad (8)$$

Pseudo first-order kinetic model equation.

$$t/qt = 1/k_2 qe^2 + 1/qe.t. \quad (9)$$

Pseudo second-order kinetic model equation. In these equations; *qe*: the adsorption capacity, k_1: the rate constant of the pseudo-first-order kinetic model, k_2: the rate constant of the pseudo-second-order kinetic model.

2.7 | Desorption experiments

Batch systems were used in the desorption processes for the purpose of evaluating the reuse efficiency. The GO adsorbent was added to the experimental tubes containing 10 ml HCl, NaOH, and ethyl alcohol (each one, 0.1 mol L^{-1}) solutions and agitate at 150 rpm for 24 h. The solutions were centrifuged at 5000 rpm for 10 min and the dye concentration in the supernatant was measured by UV–vis spectrophotometric method.

% Desorption was calculated with Equation (10).

$$\text{Desorption}\% = (q_{des}/q_{ads}) \times 100. \quad (10)$$

In these equations; q_{des}; desorbed amount of MB (mg/g), q_{ads}; adsorbed amount of MB (mg/g).

3 | RESULTS AND DISCUSSION

3.1 | The effect of adsorbent type

In this study GO and RGO were used as adsorbents for the removal of MB dye from an aqueous solution. As seen in Figure 1, GO showed maximum decolorization activity. It was reported that GO had a huge surface area and oxygen-containing groups on its surface.[37] The number of oxygens on the GO surface is more than on the surface of RGO and the surface charge becomes negative. This situation encourages the attraction of MB cations on the surface of GO. The MB dye removal percentage by GO was found the best in this study (Figure 1). Sharma et al.[38] reported that the π–π stacking formation occurred between GO and MB dye.

3.2 | The effect of initial dye concentration

The initial dye concentration is another parameter that influences the adsorption efficiency. To determine the effect of initial dye concentration on adsorption, the variety of dye concentrations were tested in the range from 25 to 400 mg/L in this study. Figure 2 indicated the results of the effect of dye concentration on the dye adsorption rate experiments, the decolorization rate was decreased by increasing dye concentration. Recently, El-Sharkaway et al.[12] reported that the MB dye removal by using polyaniline/GO percentage was decreased with the increasing dye concentration. Similar results were obtained in this study and these results were considered that the saturation on the surface adsorption sites of GO responsible for the decline of decolorization rate.

3.3 | The effect of pH

pH is an important parameter in the adsorption process. To examine the effect of solution pH on decolorization, the solution pH was set with varied pH values such as

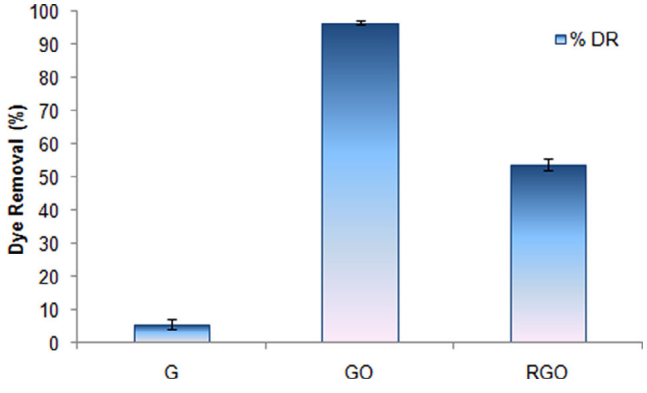

FIGURE 1 The effect of adsorbent type

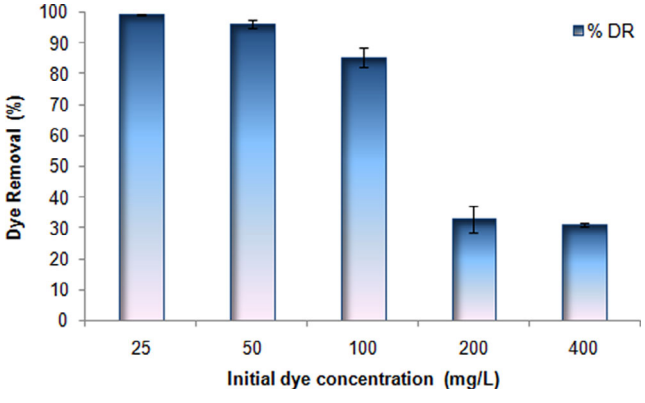

FIGURE 2 The effect of initial dye concentration

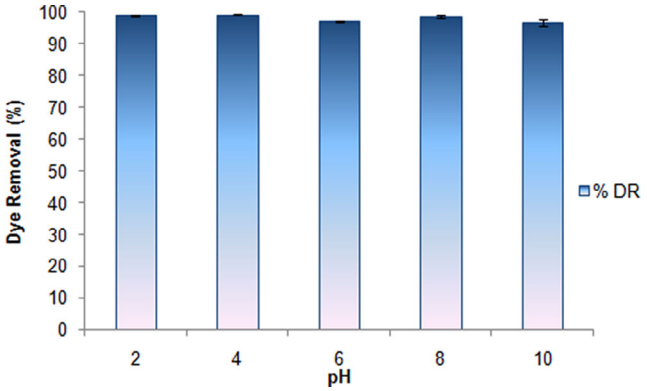

FIGURE 3 The effect of pH

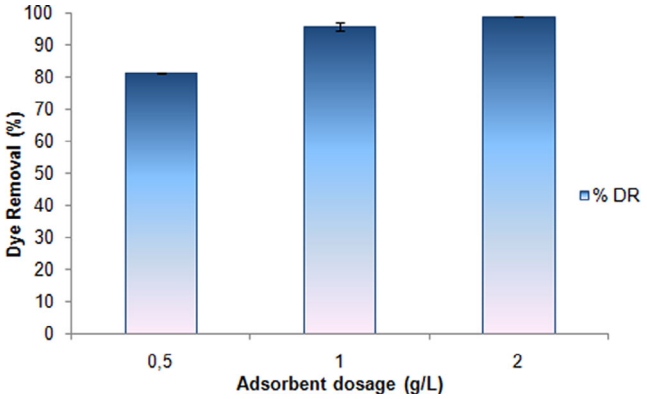

FIGURE 4 The effect of adsorbent dosage

2, 4, 6, 8, and 10 used in the experiments. While Figure 3 examined, the decolorization rates were very closed. The pH did not affect the adsorption process. El-Sharkaway et al.[12] showed that the maximum MB removal by polyaniline/GO occurred at pH 7–9 (neutral and basic pH values). In this study, the natural solution pH (at about pH 7) was selected to continue other experiments.

3.4 | The effect of adsorbent dosage

The influence of adsorbent dosage was also examined with the different amounts of adsorbent (0.5, 1, and 2 g/L). The dye removal rate was increased by increasing the adsorbent dosage (Figure 4). Recently, Othman et al.[39] demonstrated that the MB dye removal percentage was increased with the increment of adsorbent called magnetic GO owing to the increase of active sites on the adsorbent surface.

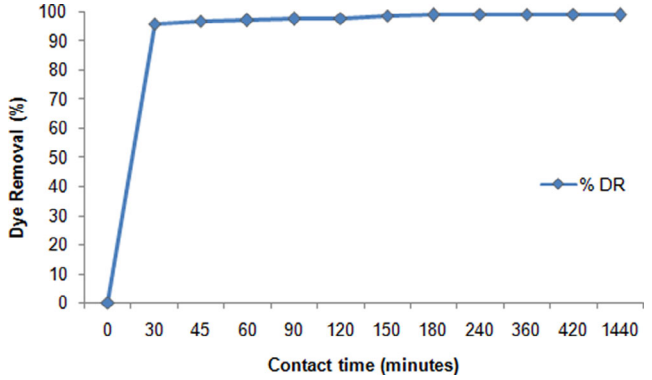

FIGURE 5 The effect of contact time

3.5 | The effect of contact time

The efficiency of the adsorption process is dependent on the optimal time because the rapid occurrence of this process saves both time and cost.[40] Figure 5 illustrates the effect of contact time on dye removal by GO. The dye removal percentage was 95.68% within 30 min and the equilibrium was found at 240 min. as 99.12% (Equation (1); Figure 5). Also, it was observed that the MB removal was rapid at the beginning and after that slowing down continuously due to the saturation of the adsorbent surface. This fast equilibrium rate probably depended on the absence of internal diffusion resistance.[41]

3.6 | Adsorption isotherms

Adsorption isotherm models were calculated at maximum decolorization environment with optimal conditions. The Langmuir and Freundlich isotherm correlation values were calculated as 0.999 and 0.949 for the adsorption of dye, respectively (Table 1). Besides, the adsorption isotherm graphics are given in Figure 6. The *qm* value indicating the adsorption capacity from the Langmuir constants as 71.43 and the K_L value indicating the adsorption energy, were found as 1.399 L/mg (Equations (2), (3), and (4); Table 1). The adsorption was suitable with the Langmuir isotherm model due to the highest correlation value. Similarly, Alhujaily et al.[42] indicated that the anionic textile dye biosorption by a cationic surfactant-modified mushroom waste was best fitted with the Langmuir model. The Langmuir isotherm model shows the homogeneous surface of the biosorbent covering with a single layer. Also, the adsorption energy was found to be 9.38 kJ mol^{-1} according to the D-R

TABLE 1 Adsorption isotherm parameters for the adsorption of MB on graphene-based adsorbent (*qm*: The maximum dye uptake per unit mass of adsorbent, K_L: Langmuir isotherm constant; K_F: Freundlich isotherm constant; MB: methylene blue; X_{DR}: adsorption capacity, K_{DR}: a measure of activity coefficient; E: adsorption free energy)

Langmuir			Freundlich			Dubinin-Raduskevich			
Qmax (mg/g)	K_L (L/mg)	R^2	K_F (L/mg)	1/n	R^2	X_{DR}	$-K_{DR} \times 10^6$	E (kJ Mol^{-1})	R^2
71.43	1.399	0.999	71.307	0.021	0.949	3.94	5.68	9.38	0.999

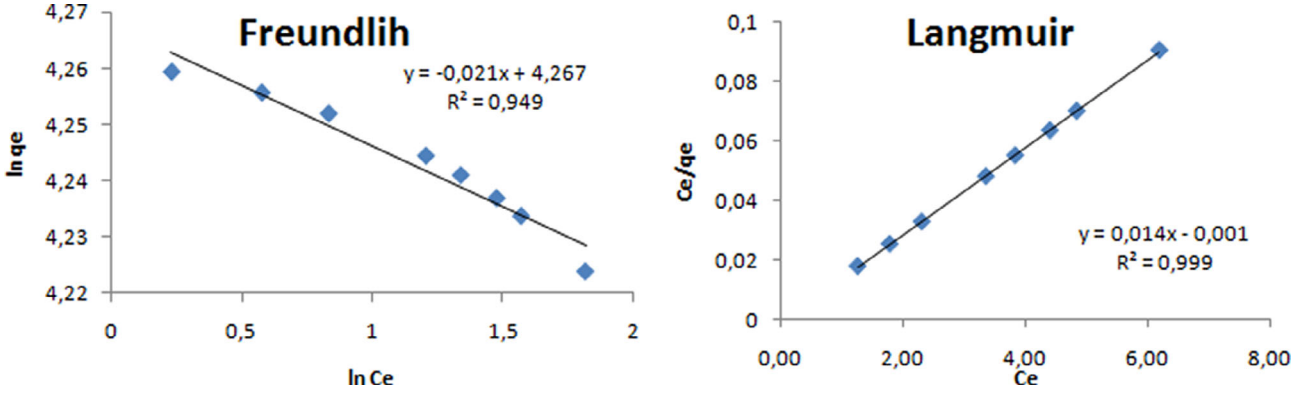

FIGURE 6 Adsorption isotherm graphics

model calculation, which indicated that the adsorption process was chemical (Equations (5)–(7); Table 1).

3.7 | Adsorption kinetics

Adsorption kinetic models were calculated from the data obtained at optimal conditions. The calculations about adsorption kinetics are given in Table 2. The graphics of adsorption kinetics are given in Figure 7. The correlation value of the pseudo-second-order model was the highest as 0.999 (Table 2), so the adsorption of MB on the GO was fitted with the pseudo-second-order kinetic model (Equation (9)). The pseudo-first-order model correlation was calculated as 0.946 which was a high value but on the other hand the difference between experimental q_{eexp} value (11.63 mg/g) calculated q_{ecal}. (71.43 mg/g) was also high (Equation (8)). The correlation of the pseudo-second-order model was high as 0.999 and the experimental and calculated qe values were very close as 71.43 and 71.428 mg/g, respectively (Table 2). The MB adsorption on the GO was fitted with the pseudo-second-order kinetic model. Similarly, Chaleshtori et al.[43] reported that the pseudo-second-order kinetic model was compatible with the adsorption of Acid Red 18 dye on activated charcoal prepared from the almond shell. Also, a recent study exhibited that the dye adsorption process by surfactant-coated mushroom waste was described by the pseudo-second-order kinetic model.[42]

TABLE 2 Kinetic parameters for the adsorption of MB onto graphene-based adsorbent (q_{ecal}: the theoretical adsorption capacity; q_{eexp}: the experimental adsorption capacity; k_1: rate constant of the pseudo-first-order kinetic model, k_2: rate constant of the pseudo-second-order kinetic model)

Pseudo-first-order model			
q_{ecal}	q_{eexp}	k_1	R^2
11.63232	71.43	0.06909	0.946
Pseudo-second-order model			
q_{ecal}	q_{eexp}	k_2	R^2
71.428	71.43	3.457	0.999

3.8 | Biosorption-desorption performance

The re-use of adsorbent is very important issue to make the adsorption process more economical. Reusability investigated the desorption ability for MB onto GO adsorbent. The GO adsorbent was renovated HCl, NaOH, and ethyl alcohol (the most common solutions used in desorption studies). The results are shown in Figure 8. Due to the results of recovery experiments, the maximum desorption capacity was examined with the ethyl alcohol (10.05%) solution. The minimum recovery percentage for MB onto GO adsorbent was obtained with HCl (7.70%).

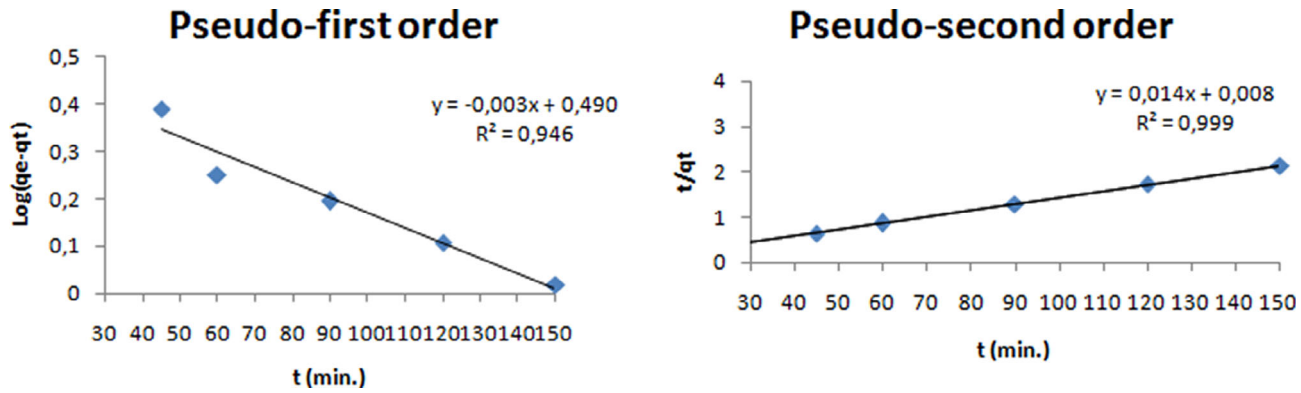

FIGURE 7 Adsorption kinetic graphics

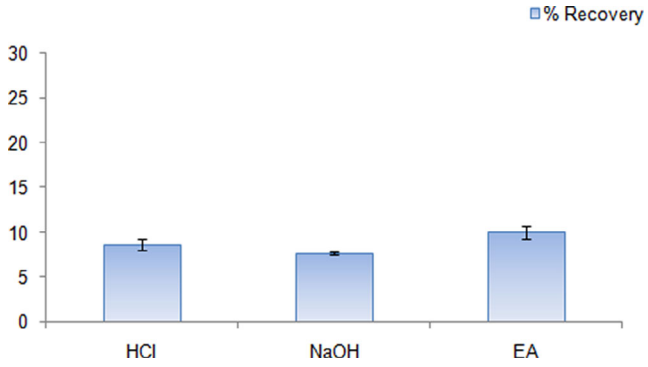

FIGURE 8 The percentage of the recovery in various solvents for desorption of MB ions. MB, methylene blue

3.9 | FTIR analysis

The structure of the GO and MB-GO interactions was investigated by the FTIR analysis. The FTIR spectra and wavenumbers of samples are shown in Figure 6 and Table 3, respectively. The FTIR analysis detected various functional groups on the surface of GO and MB-GO samples. The FTIR spectrum of GO in Figure 6 was presented the existence of functional groups such as the hydroxyl (O—H), the carbonyl (C═O), the carboxylic acid (C—OH), and the epoxy groups (C—O). For the FTIR spectrum of GO, the wide peak at 3186.99 cm^{-1} could be attributed to the O—H stretching vibrations of the adsorbed water molecules.[44] The peaks at 1713 and 1369 cm^{-1} were due to the C═O carbonyl group and the C—O—C band.[45] As can be examined in Figure 9, the bands at the wavenumbers of 1215.83 and 1035.74 cm^{-1} are assigned to C—O vibration in epoxy and C—OH vibration in carboxylic acid groups, respectively.[46] These results confirmed that GO had the oxygen-containing functional groups.[36] The results of the FTIR analysis indicated that the GO sample possessed the high-intensity characteristic peaks compared to the MB-GO sample. As seen in Table 3, some peaks were shifted, disappeared, and new peaks were also detected. The peak at 3186.99, 1713.55, 1215.83, and 1035.74 cm^{-1} corresponding to hydroxyl groups (O—H), carbonyl groups (C═O), epoxy groups (C—O), and carboxylic acid groups (C—OH) bands shifted to 3210.13, 1719.05, 1222.56, and 1039.90 cm^{-1} after adsorption, respectively. In addition, there were many new peaks in Figure 9, such as 1611.15, 1326.92, and 1379.74 cm^{-1} which are corresponding to the C═C, S═O, and C═N vibrations of the MB-GO sample. Also, C═O carbonyl and C—O—C groups of GO disappeared after adsorption by the MB since these bonds caused the appearance of the C═C bond. These FTIR results confirmed that the MB molecules have been grafted on the GO successfully.[39,46]

3.10 | XRD analysis

XRD was used to determine the crystalline structures of the GO before MB adsorption and MB-GO after MB adsorption as shown in Figure 10. XRD pattern of the GO in Figure 10 showed a peak at 9.95° with a d-spacing of about 0.82 nm according to Bragg's equation. This d-spacing was owing to the presence of oxygen-containing functional groups that increase the spacing between GO layers.[47] These results showed that the accomplished synthesis of the GO from G by the Hummers method.[48] For the XRD patterns of MB-GO, the comparatively wide diffraction peak centers at 5.17° with 1.70 nm d-spacing. There was an apparent shift in the XRD peak position from 9.95° to 5.17° and the distance between layers increased from 0.82 to 1.70 nm after MB adsorption. These results indicated the dye adsorption and confirmed the attachment of MB onto GO. Similar results were previously reported and evaluated.[49–50] Because after adsorption of dye, the characteristic peaks shift to lower

IR peak	Frequency (cm^{-1}) Before adsorption	After adsorption	Assignment Bonded groups
1	3186.99	3210.13	—OH
2	1713.55	1719.05	C—O stretching
3	–	1611.15	C—C stretching
4	1590.63	–	C—O stretching
5	–	1326.92	S—O stretching
6	–	1379.74	C—N stretching
7	1369.64	–	C—O—C stretching
8	1215.83	1222.56	C—O stretching
9	1035.74	1039.90	C—OH stretching

TABLE 3 Vibrational modes and wavenumbers of GO and MB-GO

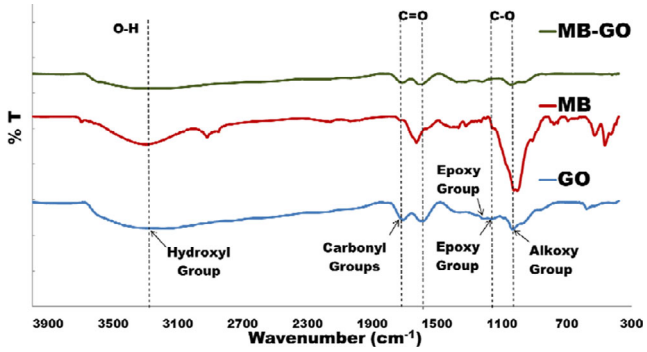

FIGURE 9 The FTIR spectra of GO, MB, and MB-GO. GO, graphene oxide; MB, methylene blue

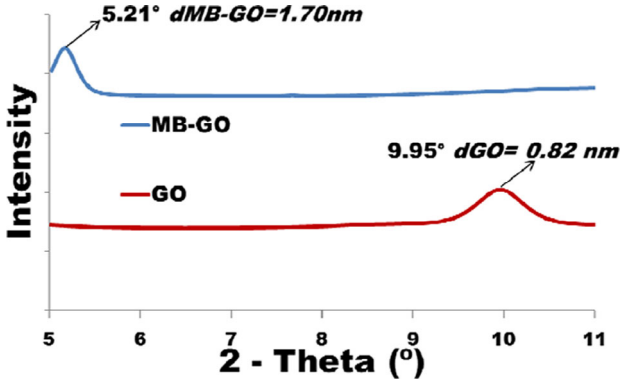

FIGURE 10 XRD patterns of GO, MB, and MB-GO. GO, graphene oxide; MB, methylene blue; XRD, X-ray diffraction

2θ values, and interlayer spacing increases. Furthermore, the full width at half maximum (FWHM) measured on the reflection (for GO 29.95°, for MB-GO 5.17°) was used in the determination of the crystallite size of GO and MB-GO samples, according to Scherrer's Equation.[51] The provided values of the crystallite size of GO and GO-MB were 14.73 nm and 29.91 nm. It was observed that MB-GO results in an increase of crystallite size achieving 202.05%, for comparison with GO. The increase in the crystallite size of MB-GO could be explained that the layered structure of GO changed completely during adsorption. In addition, the structural properties of the MB-GO will be discussed by using SEM images.

3.11 | SEM analysis

The SEM images of the GO and MB-GO samples are shown in Figure 11. From the low-magnified image of GO shown in Figure 11, it was clear that large sheets of GO had a smooth surface. The worm-like structure was observed on the surface of GO as shown in the highly magnified image. In the low-magnified SEM image of MB-GO, MB agglomerated on the sheets of GO and the highly magnified image of MB-GO in Figure 11 indicated that it had the wrinkled structure compared to GO which favors the π–π stacking interaction (adsorption) between the aromatic rings of MB molecules and GO sheets. Molla et al.[46] and Othman et al.[39] presented the same structural images for dye adsorption on GO.

The elemental analysis of GO as well as the prepared MB-GO samples were investigated using EDS (Figure 12). MB-GO sample showed a lower oxygen content with 30.12% (at. %) compared to GO. This could be attributed to the fact that C═O carbonyl and C—O—C groups of GO were reduced to MB-GO during the adsorption by the MB, as confirmed by FTIR (Figure 9). The chlorine and sulfur elements from the structure of MB appeared from the same analysis results. These results also showed the diffusion of MB molecules onto the GO. To better elaborate this adsorption mechanism, a schematic diagram is proposed in Figure 13. From the

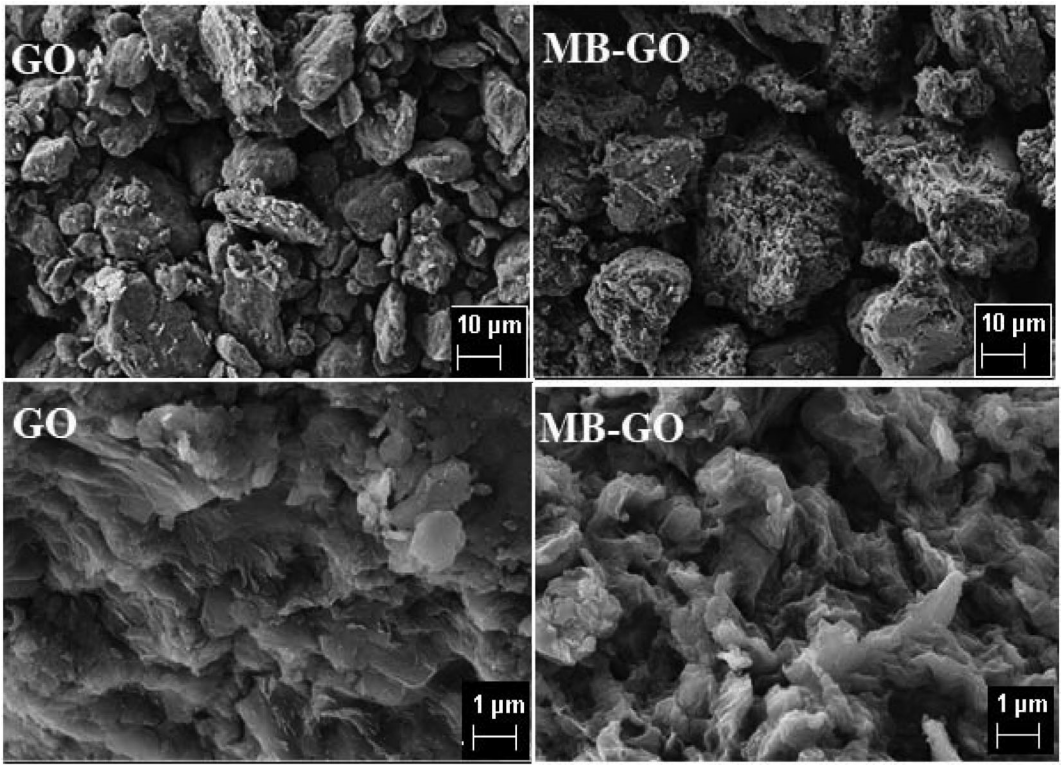

FIGURE 11 SEM images of GO and MB-GO (magnification 500 X and 5.00 KX). GO, graphene oxide; MB, methylene blue; SEM, scanning electron microscopy

FIGURE 12 EDS spectra of GO and MB-GO. EDS, GO, graphene oxide; MB, methylene blue

GO

Element	Series	unn. C [wt.%]	norm. C [wt.%]	Atom. C [at.%]	Error (1 Sigma) [wt.%]
Carbon	K-series	46.07	46.07	53.22	8.85
Oxygen	K-series	53.93	53.93	46.78	10.70
	Total:	100.00	100.00	100.00	

MB-GO

Element	Series	unn. C [wt.%]	norm. C [wt.%]	Atom. C [at.%]	Error (1 Sigma) [wt.%]
Carbon	K-series	62.07	62.07	69.12	11.15
Oxygen	K-series	36.03	36.03	30.12	8.49
Chlorine	K-series	0.76	0.76	0.29	0.12
Sulfur	K-series	1.14	1.14	0.48	0.14
	Total:	100.00	100.00	100.00	

FTIR and SEM analyses, electrostatic interactions and π-π interactions between the MB and GO were reported. Also, these electrostatic interactions were present between the N—H and S—Cl groups of MB molecules and carboxyl (COOH) groups at the sheet edges, hydroxyl (—OH) groups on the basal plane of GO, and Figure 13.[46] Also, the D-R adsorption kinetic model results represented that the adsorption of MB on the GO occurred chemically. The results obtained from all analyses proved that electrostatic interactions between MB and GO played a prominent role in the adsorption process.

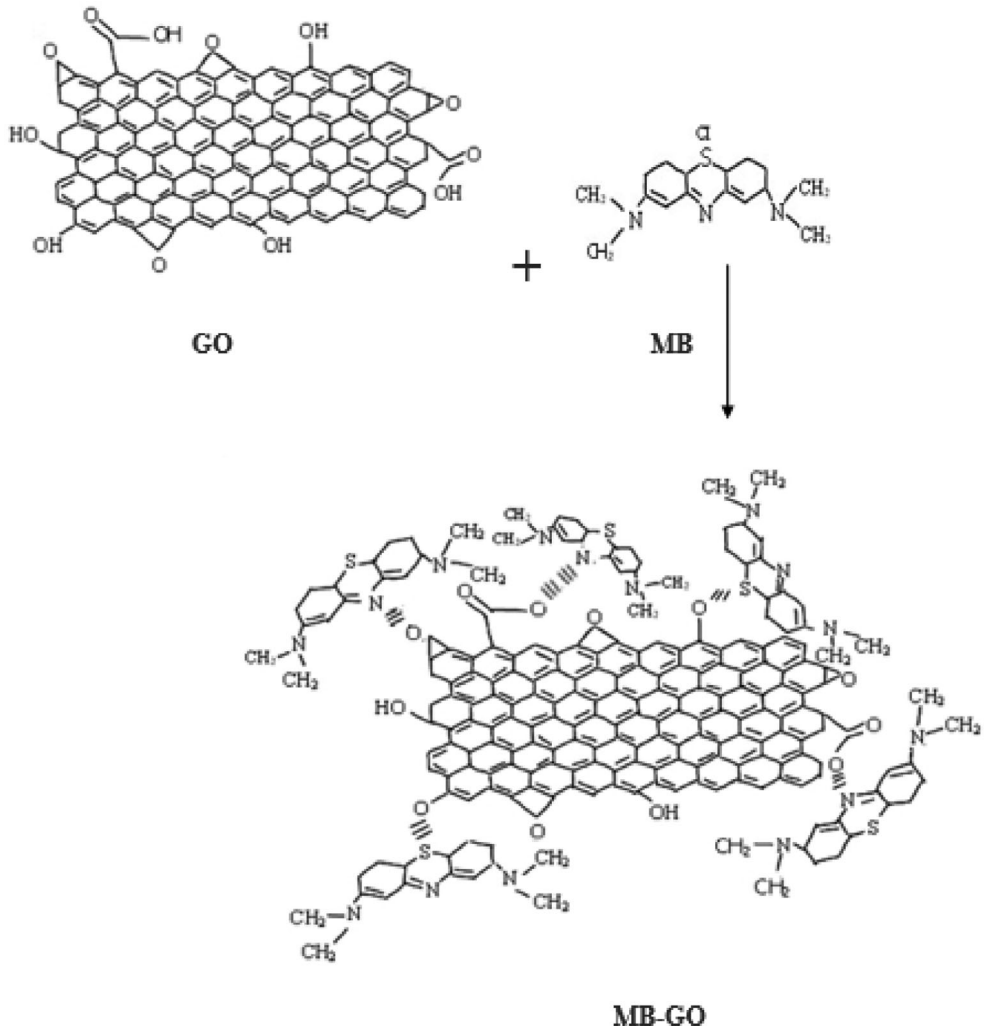

FIGURE 13 The schematic diagram of the diffusion of dye molecule onto the adsorbent

4 | CONCLUSIONS

The cationic dye removal capacities of graphene derivates (G, GO, and RGO) were investigated in this manuscript. The GO provided maximum MB dye removal among G and RGO due to its negative nature. The optimal conditions for MB removal by GO were also determined and maximum dye removal was found as 99.12% at optimal conditions. The adsorption of MB by GO was suitable with pseudo-second-order kinetic model and Langmuir isotherm. Also, the D-R model showed that the adsorption occurred chemically. To characterize the GO adsorbent XRD, FTIR, and SEM analyses were done. The obtained results of this study concluded that GO was an effective and efficient adsorbent for the removal of cationic dyes such as MB. Thanks to this study, the selection of graphene derivatives can be provided for the treatment of dye-polluted water resources.

ACKNOWLEDGMENTS

The authors acknowledge the Biotechnology Application and Research Center of Bilecik S. E. University for providing the laboratory facility.

CONFLICT OF INTEREST

The authors declare that they have no conflict of interest.

ORCID

Ferda Mindivan https://orcid.org/0000-0002-6046-2456

REFERENCES

[1] A. Imran, C. K. Jain, *Curr. Sci.* **1998**, *75*(10), 1011.
[2] M. Dehghani, M. Nozari, A. Fakhraei Fard, M. Ansari Shiri, N. Shamsedini, *Environ. Technol.* **2019**, *40*(13), 1705. https://doi.org/10.1080/09593330.2018.1428228.
[3] A. A. Basheer, *Chirality* **2017**, *30*(4), 402. https://doi.org/10.1002/chir.22808.
[4] A. A. Basheer, A. Imran, *Chirality* **2018**, *30*, 1088. https://doi.org/10.1002/chir.22989.

[5] A. A. Basheer, *J. Mol. Liq.* **2018**, *261*, 583. https://doi.org/10.1016/j.molliq.2018.04.021.
[6] A. Imran, V. K. Gupta, H. Y. Aboul-Enein, *Electrophoresis* **2005**, *26*, 3988. https://doi.org/10.1002/elps.200500216.
[7] I. Ali, O. M. L. Alharbi, Z. A. Alothman, A. Y. Badjah, *Photochem. Photobiol.* **2018**, *94*(5), 935. https://doi.org/10.1111/php.12937.
[8] P. Sharma, M. R. Das, *J. Chem. Eng. Data* **2012**, *58*, 151. https://doi.org/10.1021/je301020n.
[9] Q. He, P. Ruan, Z. Miao, K. Wan, M. Gao, X. Li, S. Huang, *Environ. Technol.* **2019**, *12*, 1. https://doi.org/10.1080/09593330.2019.1675774.
[10] A. Lunhong, J. Jing, *Chem. Eng. J.* **2012**, *192*, 156. https://doi.org/10.1016/j.cej.2012.03.056.
[11] C. Manera, A. P. Tonello, D. Perondi, M. Godinho, *Environ. Technol.* **2019**, *40*(21), 2756. https://doi.org/10.1080/09593330.2018.1452984.
[12] E. A. El-Sharkaway, R. M. Kamel, I. M. El-Sherbiny, S. S. Gharib, *Environ. Technol.* **2020**, *41*(22), 2854. https://doi.org/10.1080/09593330.2019.1585481.
[13] A. Imran, O. M. L. Alharbi, Z. A. Alothman, A. M. Al-Mohaimeed, A. Alwarthan, *Environ. Res.* **2019**, *170*, 170. https://doi.org/10.1016/j.envres.2018.12.066.
[14] I. Ali, *J. Mol. Liq.* **2018**, *271*, 677. https://doi.org/10.1016/j.molliq.2018.09.021.
[15] R. Zambare, X. Song, S. Bhuvana, J. S. Antony Prince, P. Nemade, *ACS Sustainable Chem. Eng.* **2017**, *5*(7).
[16] M. Rafatullah, O. Sulaiman, R. Hashim, A. Ahmad, *J. Hazard. Mater.* **2010**, *177*(1-3), 70. https://doi.org/10.1016/j.jhazmat.2009.12.047.
[17] M. Rafatullah, O. Sulaiman, R. Hashim, A. Ahmad, *Hazard Mater.* **2010**, *177*. https://doi.org/10.1016/j.jhazmat.2009.12.047.
[18] S. Haque, S. Gain, K. Gupta, U. C. Ghosh, *Water Qual. Res. J.* **2019**, *54*(1), 57. https://doi.org/10.2166/wqrj.2018.017.
[19] I. Ali, O. M. L. Alharbi, A. Tkachev, E. Galunin, A. Burakov, V. A. Grachev, *Environ. Sci. Pollut. Res.* **2018**, *25*(8), 7315. https://doi.org/10.1007/s11356-018-1315-9.
[20] X. J. Lee, B. Y. Z. Hiew, K. C. Lai, L. Y. Lee, S. Gan, S. Thangalazhy-Gopakumar, S. Rigby, *J. Taiwan Inst. Chem. E.* **2019**, *98*, 163. https://doi.org/10.1016/j.jtice.2018.10.028.
[21] M. Tahriri, M. Del Monico, A. Moghanian, M. Tavakkoli Yaraki, R. Torres, A. Yadegari, L. Tayebi, *Mat. Sci. Eng. C* **2019**, *102*, 171. https://doi.org/10.1016/j.msec.2019.04.051.
[22] G. Potsi, A. B. Bourlinos, V. Mouselimis, K. Poláková, N. Chalmpes, D. Gournis, S. Kalytchuk, O. Tomanec, P. Blonski, M. Medved, P. Lazar, M. Otyepka, R. Zbořil, *Appl. Mater. Today* **2019**, *17*, 112. https://doi.org/10.1016/j.apmt.2019.08.002.
[23] J. Wang, X. Jin, C. Li, W. Wang, H. Wu, S. Guo, *Chem. Eng. J.* **2019**, *370*, 831. https://doi.org/10.1016/j.cej.2019.03.229.
[24] D. Robati, M. Rajabi, O. Moradi, F. Najafi, I. Tyagi, S. Agarwal, V. K. Gupta, *J. Mol. Liq.* **2016**, *214*, 259. https://doi.org/10.1016/j.molliq.2015.12.073.
[25] P. Ranjan, P. Verma, S. Agrawal, T. R. Rao, S. K. Samanta, A. D. Thakur, *Mater. Chem. Phys.* **2019**, *226*, 350. https://doi.org/10.1016/j.matchemphys.2019.01.047.
[26] A. Arabpour, S. Dan, H. Hashemipour, *Arab. J. Chem.* **2021**, *14*(3), 103003. https://doi.org/10.1016/j.arabjc.2021.103003.
[27] W. H. Ferreira, L. G. A. Silva, B. C. S. Pereira, R. F. Gouvêa, C. T. Andrade, *Environ. Nanotechnol. Monit. Manag.* **2020**, *14*, 100373. https://doi.org/10.1016/j.enmm.2020.100373.
[28] L. Jiang, Y. Wen, Z. ZhuX. Liu, X. Liu, W. Shao, *Chemosphere* **2021**, *265*. https://doi.org/10.1016/j.chemosphere.2020.129169.
[29] A. Rohaizad, S. Shahabuddin, M. M. Shahid, N. M. Rashid, Z. A. M. Hir, M. M. Ramly, K. Awang, C. W. Siong, Z. Aspanut, *J. Environ. Chem. Eng.* **2020**, *8*(4), 103955. https://doi.org/10.1016/j.jece.2020.103955.
[30] M. H. Calimli, M. S. Nas, H. Burhan, S. D. Mustafov, Ö. Demirbas, F. Sen, *J. Mol. Liq.* **2020**, *309*, 113171. https://doi.org/10.1016/j.molliq.2020.113171.
[31] Z. Wang, M. Gao, X. Li, J. Ning, Z. Zhou, G. Li, *Mater. Sci. Eng. C* **2020**, *108*. https://doi.org/10.1016/j.msec.2019.110196.
[32] J. Xu, S. Li, F. Wang, Z. Yang, H. Liu, *J. Chem. Eng. Data* **2019**, *64*(4). https://doi.org/10.1021/acs.jced.9b00022.
[33] K. D. Lokhande, D. A. Pethsangave, D. K. Kulal, S. Some, *ChemistrySelect* **2020**, *5*(27), 8062. https://doi.org/10.1002/slct.202002130.
[34] D. A. Pethsangave, R. V. Khose, P. H. Wadekar, D. K. Kulal, S. Some, *ChemistrySelect* **2020**, *5*(4), 1516. https://doi.org/10.1002/slct.201903966.
[35] W. S. Hummers, R. E. Offeman, *J. Am. Chem. Soc.* **1958**, *80*(6), 1339. https://doi.org/10.1021/ja01539a017.
[36] F. Mindivan, M. Göktaş, *Polym. Bull.* **2020**, *77*(4), 1929. https://doi.org/10.1007/s00289-019-02831-x.
[37] Y. Zhang, J. Zhang, X. Huang, X. Zhou, H. Wu, S. Guo, *Small* **2012**, *8*. https://doi.org/10.1002/smll.201101695.
[38] P. Sharma, N. Hussain, D. J. Borah, M. R. Das, *J. Chem. Eng. Data* **2013**, *58*. https://doi.org/10.1021/je400743r.
[39] N. H. Othman, N. H. Alias, M. Z. Shahruddin, N. F. Abu Bakar, N. R. Nik Him, W. J. Lau, *J. Environ. Chem. Eng.* **2018**, *6*. https://doi.org/10.1016/j.jece.2018.04.024.
[40] E. Nazarzadeh Zare, M. Mansour Lakouraj, A. Ramezani, *New J. Chem.* **2016**, *40*(3), 2521. https://doi.org/10.1039/c5nj02880a.
[41] W. Zhang, C. Zhou, W. Zhou, A. Lei, Q. Zhang, Q. Wan, B. Zou, *Bull. Environ. Contam. Toxicol.* **2011**, *87*, 86. https://doi.org/10.1007/s00128-011-0304-1.
[42] A. Alhualiy, H. Yu, X. Zhang, F. Ma, *Int. J. Environ. Res. Public. Health* **2018**, *15*(7), 1421. https://doi.org/10.3390/ijerph15071421.
[43] A. A. N. Chaleshtori, F. M. Meghadddam, M. M. Sadeghi, R. R. Rohollah, S. Hemati, A. A. Ahmadi, *J. Environ. Sci. Manag.* **2017**, *20*(2), 916.
[44] R. Al-Gaashani, A. Najjar, Y. Zakaria, S. Mansoura, M. A. Atieh, *Ceram. Int.* **2019**, *45*(11), 14439. https://doi.org/10.1016/j.ceramint.2019.04.165.
[45] M. M. Alrashed, M. D. Soucek, S. C. Jana, *Prog. Org. Coat.* **2019**, *134*, 197. https://doi.org/10.1016/j.porgcoat.2019.04.057.
[46] A. Molla, Y. Li, B. Mandal, S. G. Kang, S. H. Hur, J. S. Chung, *Appl. Surf. Sci.* **2019**, *464*, 170. https://doi.org/10.1016/j.apsusc.2018.09.056.
[47] A. Bhattacharyya, B. Banerjee, S. Ghorai, D. Rana, I. Roy, G. Sarkar, N. R. Saha, S. De, T. K. Ghosh, S. Sadhukhan, D. Chattopadhyay, *Int. J. Biol. Macromol.* **2018**, *116*, 1037. https://doi.org/10.1016/j.ijbiomac.2018.05.069.
[48] F. Mindivan, *Mach. Technol. Mater.* **2016**, *10*(6), 32. https://stumejournals.com/journals/mtm/2016/6/32.

[49] A. Belbel, M. Kharroubi, J.-M. Janot, M. Abdessamad, A. Haouzi, I. K. Lefkaier, S. Balme, *Colloids Surf., A* **2018**, *558*, 219. https://doi.org/10.1016/j.colsurfa.2018.08.080.
[50] R. K. S. Rathour, J. Bhattacharya, A. Mukherjee, *J. Mol. Liq.* **2019**, *282*, 606. https://doi.org/10.1016/j.molliq.2019.03.020.
[51] C. Puri, G. Sumana, *Appl. Clay Sci.* **2018**, *166*, 102. https://doi.org/10.1016/j.clay.2018.09.012.

AUTHOR BIOGRAPHIES

Assistant Prof. Dr. Ferda Mindivan, born in 1983, graduated from Ataturk University, Erzurum, Turkey, Department of Chemistry, in 2005. After receiving her PhD degree from the same university in the field of Physical Chemistry in 2013, she is continuing her professional career as assistant professor in the Bioengineering Department, Bilecik Şeyh Edebali University, Bilecik, Turkey. Her main research interests are biomaterials and their structural, thermal and mechanical characterizations.

Assoc. Prof. Dr. Ülküye Dudu Gül was graduated from the biology department of Ankara University, where she was also awarded her PhD During her master's degree studies, she completed an internship program at Iowa State University in the United States as a Fulbright Scholar. She is currently an associate professor at Bilecik Seyh Edebali University. Her research interests are environmental education, environmental biotechnology, wastewater treatment technology, biosorption, bioremediation, surfactants, microbiology, industrial microbiology, mycology and algae technology.

Meryem Göktaş was born in Malatya on May 24, 1982. She received the B.Sc. degree in Mining Engineering from Inönü University, Malatya, Turkey in 2003, and M.S. degree in Mining Engineering from Dokuz Eylül University, Izmir, Turkey in 2007, and PhD degree in Mining Engineering from Inönü University, Malatya, Turkey in 2013. Since 2017, she has been working as an assistant professor of Metallurgy Department at Bilecik Seyh Edebali University, Bilecik, Turkey. Her main research interests include physicochemical operations and mechanochemical proseses in mineral engineering, graphene derivatives, polymer matrix composites and their characterization.

How to cite this article: Mindivan F, Gül ÜD, Göktaş M. Application of graphene-based adsorbents in the treatment of dye-contaminated wastewater; kinetic and isotherm studies. *J Vinyl Addit Technol*. 2021;27:485–496. https://doi.org/10.1002/vnl.21821